

34 Basaltic eruptions commonly emit both lava and pyroclasts. Often these products are produced
35 simultaneously or alternate between the two (e.g., 1959–60 eruption of Kīlauea volcano, Hawai‘i,
36 Richter et al. 1970; 1991 eruption of Hekla, Iceland, Gudmundsson et al. 1992; see Pioli et al.
37 2009). Coarse molten pyroclasts can coalesce at the base of a fire fountain and flow away as lava
38 (Parcheta et al. 2012) at the same time as fine pyroclasts are thermally lofted into a drifting ash
39 plume (e.g., Lopez et al. 2014), or ballistically carried far enough to fall as solids. Basaltic eruptions
40 can be protracted, lasting for years to decades (e.g., Miocene Roza Lava flow, Columbia River
41 Basalt Group, Thordarson and Self 1998; Pu‘u ‘Ō‘ō-Kūpaianaha, Kīlauea, Hawai‘i, Heliker et al.
42 2003; Jorullo, Mexico, Rowland et al. 2009), and can be characterised by many eruptive events
43 spread out through time and space along a fissure or amongst several vents (e.g., Fedotov et al.
44 1980; Carrecedo et al. 1992; Thordarson and Self 1993). A corollary of multi-vent eruptions is that
45 products from different vents can interact and overlap with each other to produce complex
46 stratigraphic and physical relationships (1783–85 Laki eruption, Iceland; Thordarson and Self 1993;
47 Brown et al., 2014). As a result, proximal areas around vents are dynamic, constantly changing
48 physical environments during eruptions (Holm 1987; Valentine et al. 2006; Riggs and Duffield
49 2008). Disentangling eruptive sequences in proximal regions by study of the emitted products can
50 be demanding and, for Quaternary-to-recent eruptions, is often hampered by the burial of early
51 products beneath later products (e.g., proximal pyroclastic deposits of the Laki eruption,
52 Thordarson and Self 1993). In the case of long-lived, large-volume flood basalt eruptions, lava can
53 cover hundreds to thousands of square kilometres in all directions away from a vent, and in some
54 cases almost all pyroclastic material can become buried during the course of the later stages of an
55 eruption (e.g. Brown et al. 2014).

56 Understanding the nature of these interactions can help in the piecing together of eruption
57 histories because deposits hold a wealth of information that can be used to infer eruption dynamics
58 (e.g. column heights, mass fluxes, durations, steadiness; Carey and Sparks 1986; Wilson and
59 Walker 1987; Pyle 1989; Parfitt and Wilson 1999; Houghton et al. 2006) and to elucidate landscape
60 evolution in proximal regions. However, in order to extract useful information, individual layers
61 need to be confidently traced away from the vent to construct isopachs, isopleths, and to establish
62 stratigraphic relationships. This is not always easy. Several common characteristics of basaltic
63 eruptions can reduce the confidence with which fall deposits can be traced away from source.
64 Firstly, many erupted basaltic magmas are chemically monotonous and even large-volume
65 eruptions can exhibit minimal change in geochemistry through time (e.g., Roza and Sand Hollow
66 lava flow fields, Columbia River Basalt Group, Martin 1989 and Vye et al. 2013; 1783–75 Laki
67 eruption, Iceland, Sigmarsson et al. 1991; Passmore et al. 2012). Secondly, sustained, steady phases

68 of eruptions produce pyroclastic deposits that can be massive and texturally homogeneous, and that
69 lack traceable layers.

70 In this paper our purpose is to outline some of the ways in which proximal pyroclastic fall
71 deposits can become disrupted by lavas during basaltic eruptions. We then describe some of the
72 complex physical and stratigraphic relationships that can result from these processes. We use
73 examples from historic eruptions and from the geologic record (Table 1). We discuss the
74 implications of these processes for understanding landscape evolution, eruption dynamics, and
75 emplacement mechanisms in proximal environments during basaltic eruptions. We illustrate that
76 these processes may inhibit the collection of accurate isopleth and isopach data in proximal areas
77 through the generation of allochthonous tephra deposits and through the modification of a deposit's
78 original thickness.

79

80 **Field data on disrupted basaltic fall deposits**

81 *Roza Member, Columbia River Basalt Group, USA*

82 The Roza Member in the Columbia River Basalt Group (CRBG) is a 1300 km³ flood basalt flow
83 field covering ~40300 km² of the states of Washington and Oregon (Martin 1989; Thordarson and
84 Self 1998; Fig. 1). It comprises four major lava flows and at most localities it is formed of 1–3
85 stacked sheet lobes, which together can reach over 70 m thick. The Roza dike vent system can be
86 traced for > 180 km from NE Oregon into SE Washington (Swanson et al. 1975; Brown et al.
87 2014). Proximal tephra fall deposits are exposed around fissure segments at the northern end of the
88 Roza vent system (Swanson et al. 1975; Fig. 1). Ten fissure vent localities have been recognised
89 north of the Snake River (Brown et al. 2014), over an along-strike distance of 30 km. These
90 pyroclastic rocks outcrop over minimum areas of 0.5–2 km² and are inferred to have originally
91 formed cones, ramparts and sheets comprised of scoria, densely welded spatter, spatter-fed lava and
92 spongy pāhoehoe (Swanson et al. 1975; Brown et al. 2014). Large spatter bombs constrain the
93 location of the vents to within several hundred metres and record fallout under lava fountains.
94 Cone-forming pyroclastic deposits can exceed 50 m thick and all vents were substantially buried by
95 later-emplaced Roza lava in the same prolonged eruption (Brown et al. 2014).

96 Tephra deposits are particularly well-exposed in natural and man-made sections around the
97 town of Winona, Washington State (Fig. 2; e.g. Thordarson and Self 1996; Brown et al. 2014).
98 Here, the base of the Roza Member is not exposed and the lowest Roza product is a poorly exposed
99 lava flow with the surface characteristics of rubbly pāhoehoe (e.g., Kezsthelyi et al. 2004; Guilbaud
100 et al. 2005; Duraiswami et al. 2008). It is overlain by pyroclastic deposits, the source of which is
101 inferred to be a fissure vent that is exposed in a 2D east-west oriented railway cut 500 m to the west

102 (Fig. 2). The position of the vent is constrained by two, discontinuously exposed, opposing
103 accumulations of densely welded spatter and scoria that built up on either side of a fissure (Fig. 2;
104 Brown et al. 2014). The spatter deposits generally dip at low angles away from the fissure and thin
105 from >20 m to <2 m over a horizontal distance >500 m. In proximal regions, dense welding means
106 that the outlines of constituent spatter bombs are not visible. Instead the rock appears glassy with
107 thin wispy fiamme inferred to be remnant vesicular interiors of bombs (Thordarson and Self 1996,
108 1998; Brown et al. 2014). With distance the welding intensity decreases and the outlines of spatter
109 and scoria bombs are apparent. The welding intensity appears to decrease upwards, although these
110 deposits are inaccessible. The vent is filled with a later-emplaced lava sheet lobe and the whole
111 sequence is capped by an even later 20 m thick Roza sheet lobe (Fig. 2).

112 At distances of 800–1500 m from the fissure, tephra deposits comprise non-welded, well
113 sorted ($\sigma\phi = \sim 1$), massive to weakly horizontally bedded lapilli (Thordarson and Self, 1998). The
114 fall deposits exhibit unusual geometries and stratigraphic relationships with interbedded, thin,
115 highly vesicular, and rubbly pāhoehoe lavas (Fig. 3a and b). At the base of this succession is a
116 pāhoehoe lava flow whose upper, highly vesicular crust is rubbly and consists of jumbled slabs and
117 blocks that range in size from <0.1–1.5 m (Fig. 3a). The slabs and blocks have vesicularities up to
118 50 vol. % and some exhibit ropy fluidal exteriors and sheared vesicles. Some of the larger slabs are
119 steeply to vertically oriented (Fig. 3b). The upper surface of this lava flow exhibits relief of 1–5 m
120 and is the lowest unit exposed in the area; only the topographic highs along its upper surface are
121 exposed at the base of artificial cuttings. Overlying this is a broad, smooth-surfaced mound of well-
122 sorted, poorly consolidated to unconsolidated, angular, medium lapilli tephra (up to 2 cm in
123 diameter; Fig. 3c and d). This mound is up to 4 m high and 20 m wide. The lapilli tephra fills the
124 void space between the blocks and slabs of the underlying vesicular lava crust. Draping this mound
125 of scoria is a second pāhoehoe lava flow that has been disrupted into decimetre-sized, joint-
126 bounded, angular, and vesicular blocks (Fig. 2). The lava is >3 m thick in the topographic
127 depressions on either side of the mound and thins to <30 cm thick over the top. Where the mound
128 pinches out to the east the second lava lies on top of the first. This second lava appears to be of
129 limited extent (Fig. 2 and 3). Overlying the second lava is a series of tephra mounds exposed over a
130 lateral distance of ~200 m (Fig. 2). They are similar in texture, grainsize, and composition to the
131 lower tephra mound. The tephra clasts are moderately clay altered but some pockets of pristine
132 tephra are present within the mounds: the density of the lapilli clasts ranges from 400–1200 kg/m³,
133 which equates to vesicularity values of 55–85 % using a magma density of 2700 kg/m³ (Brown et al.
134 2014). Each mound is up to 5 m thick, up to 30 m wide, and they are spaced ~25–40 m apart
135 (centre-to-centre; Table 2). They are typically massive although at some outcrops bedding is poorly

136 defined by several slightly finer-grained horizons each several centimetres thick. These mounds
137 have flat-topped, peaked or convex morphologies (Table 2) with outer slopes of 20–60°. Some
138 mounds are linked to each other but others are seemingly detached from neighbouring mounds, at
139 least in 2D (Fig. 2). In some of the mounds sub-horizontal bedding is present. The mounds all occur
140 along the same stratigraphic horizon and feature sub-horizontal bedding and are therefore taken to
141 be part of the same fall deposit (Brown et al. 2014).

142 The lava flows underlying the mounds are poorly exposed and vary considerably. At some
143 locations they are composed of lobes several metres thick and up to 50 m wide. However, at the
144 eastern end of the rail cut at Winona, three thin vesicular lava flows are interbedded with tephra fall
145 deposits (Fig. 2). Elsewhere tephra that has percolated down into tumuli in underlying lobes has
146 been thermally discoloured indicating that the underlying lava was still hot.

147 The upper mounds are draped by densely welded spatter deposits and the exteriors of the
148 mounds in contact with the spatter have been sintered to depths of 5–10 cm. The overlying deposits
149 consist of ~65 cm thick, finely crystalline, lava-like tuff with sparse spherical vesicles in its middle
150 part. Sharply overlying this unit is ~40 cm of brown glassy welded tuff with ghost fiamme typically
151 1–1.5 cm long and <1–2 mm thick. This is sharply overlain by >12 m of dense, columnar jointed
152 Roza lava. The lower two layers appear to have locally slumped on some mounds and occur twice
153 or three times as a repeating sequence; elsewhere small-scale disruption of the sequence is also
154 consistent with slumping (Fig. 2). This indicates that the mounds are larger in 3D than they appear
155 in 2D. One mound exhibits a subvertical downward-tapering crack that has been filled by Roza lava
156 from the uppermost exposed dense lava (Fig. 3c and d).

157 Discrete mounds of variably oxidised agglutinate, spatter and moderately densely welded
158 tephra outcrop on top of the uppermost Roza Member sheet lobe, at distances of <1 km from
159 inferred fissure vents (Fig. 2). They are particularly common at the western end of the railway cut at
160 Winona, where they outcrop across an area of <400 m², and are also well exposed in Mason Draw
161 (Table 1). Each mound is typically several metres high and has a cross-sectional area of several to
162 tens-of-metres square. Most comprise massive to crudely bedded and densely to moderately welded
163 spatter and scoria. Clasts reach 25 cm in diameter. Bedding and spatter clast foliation dips are
164 typically high (20–46°) and adjacent, but unconnected outcrops can exhibit strongly divergent dips
165 and strikes. This crude foliation is commonly terminated by the edges of the mounds. The lower
166 contacts with underlying sheet lobes are not exposed, but at Winona the mounds outcrop at the
167 same altitude as the underlying flow's vesicular upper crust, indicating that the upper surface of the
168 sheet lobe had several metres of relief.

169 Two larger mounds of non-welded to densely-welded pyroclastic rocks, interbedded with
170 thin rubbly pāhoehoe lava, occur 2 km north of Winona. These are up to 15 m thick, 30 m wide, and
171 are draped by 2.5 m of non-welded to moderately welded scoria fall deposit.

172

173 *Grande Ronde Member, Columbia River Basalt Group, USA*

174 Tephra fall deposits occur within the 16 Ma Grande Ronde lavas (Barry et al. 2010) at Little Sheep
175 Creek, Oregon (Table 1 and Fig. 4). They are interbedded with three lavas exposed along road cuts.
176 The upper and lower lavas comprise thick (4–8 m) sheet lobes with rubbly, vesicular upper crusts
177 that reach 5 m thick. These rubbly crusts are intruded by irregular, sub-vertical squeeze-ups of
178 blocky-jointed dense lava core that have assimilated and agglutinated rubble onto their exteriors.
179 Contacts with the rubble are glassy or gradational. The middle lava is overlain by a 10 m-thick
180 scoria fall deposit exposed in a 150 m-long road cut (part of which is shown in Fig. 4). At this
181 location only the brecciated upper crust of the lava is exposed in the form of multiple sub-vertical
182 protrusions of dense lava that are similar to those that pierce the rubbly crusts of the upper and
183 lower lavas (Fig. 4). The tephra fall deposit is texturally similar to that described from the Roza
184 Member and is massive to weakly bedded (Fig. 4). The tephra is strongly altered to palagonite, but
185 the outlines of individual clasts and vesicles are still visible. The deposit is well sorted, clast-
186 supported, and comprises scoria lapilli <2 cm in diameter. The squeeze-ups of lava are 0.1–3 m
187 wide (Fig. 4) and extend upwards from an underlying sheet lobe that has a brecciated vesicular
188 upper crust composed of variably vesicular blocks of lava, similar to that of the upper and lower
189 sheet lavas. The cores of the intrusions are coherent, well-jointed, dense lava with scattered large
190 gas vesicles up to 20 cm in diameter. The upward tapering intrusions are partially encased in a
191 carapace of rubble (Fig. 4) and exhibit complex morphologies. Contacts between the rubble and the
192 intrusions vary from sharp to gradational. A tephra fall deposit in contact with the squeeze-ups has
193 been thermally oxidised to a depth of <1 m (Fig. 4). It is unclear if any protrusions reach the upper
194 surface of the scoria fall deposit, which is overlain by lava. The uppermost few decimetres of the
195 fall deposit has been oxidised by the overlying lava (Fig. 4).

196

197 *Chinyero volcano, Tenerife, Canary Islands*

198 The 1909 Chinyero eruption, Tenerife (Table 1, Fig. 5), lasted for 10 days and produced a scoria
199 cone, tephra fall deposits, and a basaltic lava flow that covered ~2.7 km² (see Carracedo 2013). At
200 least five vents were active during the lifetime of the volcano (see Carracedo 2013).

201 Field relationships indicate that the effusion of lava alternated and overlapped with the
202 development of quasi-steady eruption plumes that dispersed lapilli and ash to the northwest.

203 Significant portions of the scoria cone (blocks 8 m high) have been rafted up to 1 km from source,
204 leaving a crescent-shaped pyroclastic construct standing 80 m high around the vent area (Fig. 5). An
205 extensive ‘a‘ā lava flow field extends southwards away from the vent.

206 The lava flow field is partially covered in tephra fall deposits derived from the eruption (Fig.
207 5 and 6). Stagnant parts of the lava flow remain covered in a smooth undisrupted tephra blanket that
208 mantles the irregular surface of the lava flow. Lava that continued to flow from the vent after fallout
209 ceased disrupted the overlying tephra blanket and generated a series of rafted tephra mounds along
210 the margins of the flow (Fig. 6A, B, D). The mounds are up to 1.5 m high and have slopes of 20–
211 36° (Table 3; Fig. 6). Both isolated and connected mounds are present: isolated mounds are 2–10 m
212 apart and 3–10 m wide. The lava flowed over more distal parts of the same tephra blanket that lay
213 on top of it, resulting in a repetition of the fall deposit (Fig. 6C): the lower layer is finer-grained
214 than the rafted layer which was carried several hundred metres on top of the lava. Parts of the lava
215 flow field that post-date fallout and do not have disrupted mounds on top of them are devoid of
216 tephra cover (Fig. 6D).

217

218 *Hekla volcano, Iceland*

219 The 1991 eruption of Hekla, Iceland, began with a ~1 hour-long explosive Subplinian (initial) phase
220 that produced a ≥ 11.5 km high eruption column and a north-northeast dispersed plume with
221 significant tephra fall up to 370 km from the volcano (Gudmundsson et al. 1992). This was
222 followed by stepwise unzipping of the Hekla fissure to the southwest of the summit crater as well as
223 to the base of the eastern flank, forming a 5-km-long fountaining fissure across the volcano (Fig. 7).
224 This phase of the eruption was characterized by simultaneous explosive and lava fountain activity,
225 producing tephra-rich columns, 300–500-m-high lava fountains and fountain-fed lava flows that
226 cascaded down the western, southern and eastern slopes of the volcano, reaching lengths of 4–5.5
227 km in <6 hours. Shortly thereafter, new lava fountains emerged from radial northern and southern
228 fissures (Fig. 7). During the ~1 hour-long Subplinian summit phase the magma discharge was just
229 over 2000 m³/s, whereas during the fissure forming phase the discharge dropped abruptly to <20
230 m³/s in the course of 3 days (Gudmundsson et al. 1992). This decline in magma discharge coincided
231 with an eastward shift in the activity as well as gradual decrease in eruption intensity and
232 progressive localization of the active vents towards the eastern most part of the Hekla fissure. By
233 the third day of the eruption the activity was characterized by lava fountaining on a short (<500 m-
234 long) fissure segment at the site of the East Cone (Fig. 7). Two days later the activity was
235 characterized by a single gas jet carrying sporadic bombs to heights of several hundred-meters with
236 only minor amounts of ash. Coarse ejecta gradually piled up around the vent to form the 80-m-high

237 and ~250-m-wide East Cone. At the same time lava was discharged at rates of 1–12 m³/s, feeding
238 the ‘normal’ lava flows through several vents below the East Cone. During the first 3–4 days the
239 fissure segment, now represented by the East Cone, featured intense lava fountaining that blanketed
240 the immediate surroundings (up to 1–1.5 km from the vents) with fallout, which on the surface was
241 represented by a continuous blanket of tephra. The surface slope in this area was 5–10°.

242 Shortly thereafter, arcuate tension cracks opened up in this tephra blanket to the north and
243 east over a rectangular area of 0.15 km² (Fig. 8A). The cracks are oriented transverse to the dip of
244 the slope, 5 m wide, and up to 5–9 m deep which at the time of the eruption extended down
245 through 3–6 m of lapilli tephra fall deposit and up to 3 m of incipiently to intensely welded spatter
246 deposit into an incandescent horizon that formed the basal clastogenic lava that was still creeping
247 downslope at the time of observation by one of the authors (Thordarson) (Fig. 8B–D). As the
248 incandescent clastogenic part crept downslope, the overlying, and then unconsolidated welded
249 spatter units and unconsolidated lapilli tephra units underwent extension and broke up into series of
250 lenticular coherent blocks, each up to several metres wide and several hundred metres long (Fig. 8).
251 During downslope creep, some tephra blocks underwent small degrees of rotation, which resulted in
252 their upper surfaces dipping upslope by <15°, and therefore these may in some instances resemble
253 listric faults. Small grabens developed with vertical displacements of <1 m. The area that underwent
254 downslope creep was bound by a discontinuous head scarp (Fig. 8).

255 The overlying scoria fall deposit had a significant coherence through the interlocking of
256 angular and spinose tephra. This allowed the non-welded deposit to maintain steep, vertical and
257 slightly overhanging faces during fissure and tension-crack development and lateral spread.
258 However, small talus fans of scoria within the cracks (Fig. 8b–d) built up by collapse and grainflow
259 during or shortly after rifting. The initially vertical sides of the blocks became subdued over time as
260 material collapsed into the crevices, in many cases almost completely filling the cracks (Fig. 8).
261 Over time the jagged topography became subdued into a series of low convex ridges aligned sub-
262 parallel to the strike of the slope.

263 Examples of similar formations, comprised of a series of elongate tephra mounds and
264 underlain by clastogenic lava, although with much less jagged topography, are present in an historic
265 lava flow that crops out on the NE slopes of Hekla between the northernmost lava branches of the
266 1980 and 1991 events (Fig. 7). By the same token, similar tephra mounds crop out in the near-vent
267 region of the 1783–85 Laki eruption, namely in the south side of the Hnúta vent segment and within
268 the lava in Varmárdalur straight west of the northwest end of Galti (Table 1).

269

270 **Interpretation and discussion**

271 *Formation of the tephra mounds*

272 The examples described above illustrate how tephra fall deposits can become disrupted and
273 dissected during basaltic eruptions. The examples from the CRBG provide 2D cross-sections
274 through tephra sheets, whereas the examples from Tenerife and Iceland allow the 3D morphology
275 of the deposits to be examined.

276 The tephra deposits of the Roza Member at Winona are inferred to have been deposited at
277 distances of >800 m from a vent that is exposed in the railway cut (Fig. 2; Brown et al. 2014).
278 Truncation of sub-horizontal bedding by the edges of some mounds demonstrates that the tephra
279 deposits originally mantled the substrate as continuous sheets (Fig. 2). There are several possible
280 explanations for how these sheet-form fall deposits could have become dissected into partially
281 connected and unconnected mounds. Swanson et al. (1975) envisaged that the mounds formed due
282 to bulldozing by advancing lava flows, but this should result in chaotic mounds with severely
283 disrupted bedding. Erosion of the fall deposit by surface water is discounted due to the absence of
284 evidence for aqueous reworking (e.g., scours, rills or gullies). The high porosity and permeability of
285 the coarse-grained fall deposits, combined with the low palaeoslope angles would have inhibited
286 surface run-off.

287 Instead, we favour an interpretation whereby the tephra sheets were disrupted into mounds
288 by an underlying lava flow, which was still moving (Fig. 9), through some combination of lateral
289 (flow) and vertical (differential inflation) movement. This interpretation is backed up by the
290 similarities in morphologies and dimensions between the Roza tephra mounds and those on top of
291 the Chinyero lavas, which clearly rafted on top of a lava flow (see Figs 2 and 6; e.g., Holm 1987;
292 Valentine et al. 2006; Riggs and Duffield 2008). The underlying lavas in both cases are
293 characterised by rubbly crusts with metre-scale relief. In the Roza Member, tephra that has
294 percolated down into void spaces in the rubbly tops of the lava, and has been thermally oxidised by
295 the lava, confirms that fallout occurred on top of active lava flows. We infer that extension of the
296 tephra sheet enabled grain flow and collapse of scoria lapilli away from the separated parts of the
297 fall deposits (Fig. 9). The irregular, spiny shapes and interlocking nature of the lapilli meant that
298 free surfaces would maintain steep slope angles on the exteriors of some mounds for a short period
299 (months to years). Mounds with convex morphologies and shallower slope angles may have been
300 modified by the gravitational remobilisation of loose scoria into the depressions (e.g., by grainflow,
301 collapse): this may also indicate that a significant period (months to years) passed before they were
302 covered by younger deposits (the Roza eruption is considered to have lasted years, Thordarson and
303 Self 1998). The well-sorted nature of the tephra and the short distance (from the scarp of the

304 fracture to the bottom of the fracture) over which remobilisation operated means that it would be
305 difficult to distinguish remobilised deposits from in-situ deposits (except where bedding is present).

306 The presence of interbedded lava flows and tephra fall deposits in the Roza Member
307 indicates that effusion of lava and fallout from eruption columns was synchronous or alternated
308 during successive phases of the eruption. Some thin vesicular lava flows intercalated within fall
309 deposits may have been fed by break-outs of lava from subjacent tumuli during inflation (e.g., Fig.
310 2). Break-outs could have intruded up through the overlying tephra fall deposit and then started to
311 flow across the fall deposit's upper surface as lobes of gas-rich pāhoehoe lava (Fig. 9). Field
312 relationships indicate that they ponded within depressions between mounds (Fig. 2). The intrusions
313 into the scoria fall deposit of the Grande Ronde lavas (Fig. 4) are interpreted in a similar manner.
314 Tephra fell out on top of an active lava flow. As the underlying lava flow inflated, tumuli developed
315 and breakouts of viscous degassed lava were injected upwards through the tephra fall deposit. The
316 margins of the intrusions chilled and brecciated against the overlying enclosing fall deposit and in
317 doing so thermally oxidised it (Fig. 4). As inferred for the Roza Member, some of these intrusions
318 may have reached the surface of the tephra fall deposit and then flowed across the surface of the
319 lava flow as pāhoehoe lobes, but it currently cannot be proven from the field relationships.

320 Disruption of the tephra sheet at Hekla was achieved in a manner similar to that outlined
321 above. Here, though, viscous flow occurred in a layer of clastogenic lava beneath coherent non-
322 welded tephra fall and spatter deposits (Fig. 8). As this clastogenic lava flowed downslope, the
323 overlying fall deposit behaved as a brittle coherent mass under extension (Fig. 8). We speculate that
324 the overlying tephra deposits acted to insulate the clastogenic lava, but that once spreading
325 occurred, heat loss through open cracks and fissures may have led to higher rates of cooling and
326 may have acted to slow and eventually halt viscous flow. Similar tension cracks within scoria fall
327 deposits were observed on the shoulders of the Pu'u Ō'ō cone, Kīlauea volcano, Hawai'i (Heliker
328 et al. 2003) and on many of the cones formed during the 1783–5 eruption of Laki. At Kīlauea
329 volcano, these cracks penetrated subjacent incandescent material that was inferred to have been
330 creeping downslope (Heliker et al. 2003).

331 The spatter mounds on the tops of the Roza sheet lobes form discrete outcrops of variably
332 dipping pyroclastic material that are texturally and compositionally similar to the pyroclastic
333 deposits that form proximal vent constructs in the Roza Member (Brown et al. 2014). We infer that
334 they are the remnants of proximal constructs, such as spatter ramparts that have been rafted from
335 the vent in lava channels (see also Chinyero volcano, Fig. 6D). This differs from the other outcrops
336 described here (e.g., in the Roza Member at Winona, and at Hekla), in that the transport distance is
337 much greater, and the other outcrops record disruption of tephra sheets, rather than proximal

338 edifices. Rafted segments of pyroclastic edifices, reaching up to several hundred metres wide, have
339 been documented at other volcanoes (e.g., Holm 1987; Valentine et al. 2006; Riggs and Duffield
340 2008) and are generated when lava breaches or undermines scoria cones or spatter ramparts.
341 Because the pyroclastic material is of lower bulk density (e.g., average bulk density of 1700 kg/m^3
342 for the Roza Member, Brown et al. 2014) than the lava, it can be carried for several kilometres as
343 flotsam in open channels (Holm 1987; Riggs and Duffield, 2008). The occurrence of rafted spatter
344 ramparts over areas of $\sim 0.5 \text{ km}^2$ in the Roza Member is consistent with major breaches of proximal
345 constructs by lava.

346

347 *Implications for reconstructing stratigraphic relationship and tephra fall isopach maps for basaltic* 348 *eruptions*

349 Tephra fall deposits contain information (e.g., thickness, maximum clast size) that can be used to
350 probe and quantify the dynamics of explosive volcanic eruptions (e.g., Carey and Sparks 1986
351 Wilson and Walker 1987; Pyle 1989; Parfitt and Wilson 1999; Houghton et al. 2006). This is best
352 achieved where deposits are accessible, well preserved, well exposed, and unaffected by erosion or
353 weathering, and it becomes more difficult the more eroded or more poorly exposed a deposit is.
354 Proximal deposits are important in the construction of total grain size distributions of fall deposits,
355 which can be used to infer fragmentation and eruption style and help understand plume dynamics
356 (Bonadonna and Houghton 2005). Our observations from the USA, Tenerife, and Iceland, illustrate
357 the ways in which pyroclastic deposits can become disrupted in proximal regions during basaltic
358 eruptions, resulting in complex stratigraphical relationships between lavas and pyroclastic deposits.
359 These mechanisms include lateral and vertical displacement caused by movement of underlying
360 lavas, rafting of strata from proximal edifices atop lava flows and downslope creep and lateral
361 spread initiated by rheomorphic flow of clastogenic lava. Some of these outlined processes have
362 resulted in the repetition of fall layers (e.g., Fig. 2). Whilst these processes can be observable in the
363 products of young eruptions (Fig. 6), such relationships become difficult to recognise in poorly-
364 exposed deposits or in those in the geologic record. This can be compounded because fall deposits
365 and lavas from basaltic eruptions can show little textural, physical, or chemical variation. This
366 results in an absence of distinct marker horizons with which to correlate similar-looking sequences
367 between outcrops.

368 The relationships outlined here indicate that tephra fallout either alternated or was
369 synchronous with the emplacement of lava flow fields. These situations could arise if the lava flows
370 are fed by vigorous fountains ($>0.5 \text{ km}$ in height), or if pyroclastic material and lava are emitted
371 from separate vents along a fissure. During synchronous lava effusion and fallout, the bases and the

372 tops of tephra deposits may well be diachronous where they are in contact with advancing lava
373 flows (the tops and bases of lava flow fields are always diachronous)(Fig. 10). As an example,
374 pāhoehoe flow fields advance by successive metre to sub-metre-sized break-outs of lava at rates of
375 0.01–0.7 km/hour (e.g., Thordarson and Self 1993; Hon et al. 1994), while fallout during basaltic
376 eruptions can last for many hours to days (e.g., Rowland et al. 2009). Advancing lava will
377 transgress depochrons (cryptic lines joining particles deposited at the same time; after Branney and
378 Kokelaar, 2002) within the accumulating fall deposit. This means that that pyroclasts lying on top
379 of the lava flow field in proximal locations correlate with pyroclasts beneath that same flow field in
380 more distal locations (Fig. 10). Additionally, given that the pathways of advancing lava are
381 determined by the substrate topography and by the flow field's internal lava transport system, the
382 paving of ground by lava may be highly irregular through time and space. This is achieved by lobes
383 that split, converge, accelerate and decelerate non-uniformly and can result in the formation of
384 kipukas and lava rise pits (e.g., Walker 1991). Complex temporal and spatial relationships between
385 flow fields and any coeval tephra fall deposits may remain cryptic in the geological record. In
386 modern deposits, such relationships might not be apparent due to partial burial of fall deposits by
387 later erupted lavas. Break-outs from tumuli could feed small secondary lava flows that spread
388 across the upper surface of the fall deposit rather than the upper surface of the lava (Fig. 9). While
389 this has not been proven to have occurred in the CRBG examples, the field relationships seen there
390 (Figs 2 and 4) and observations of break-outs from modern pāhoehoe lava flows demonstrates that
391 this is possible. This would act to further complicate outcrop-scale stratigraphic relationships
392 between fall deposits and lavas in proximal environments.

393 The eruptions of Chinyero, Tenerife, only lasted for 10 days (Carrecedo 2013) while Hekla
394 continued for <8 weeks (Gudmundsson et al., 1992). The potential for the disruption of fall deposits
395 increases the longer an eruption lasts. For flood basalt eruptions, thought to last years to tens-of-
396 years (Thordarson and Self 1998; Self et al. 2006), disruption of tephra deposits due to interaction
397 with lavas is almost inevitable. Lava flows fed by effusion from one vent can inundate large areas
398 prior to the opening of another vent along the fissure, and actively inflating sheet lobes can receive
399 fallout onto their deforming upper crusts. Given that the fissure system that fed the Roza Member
400 was >180 km long, and was host to numerous vents (Brown et al. 2014), the sorts of processes
401 outlined here should be expected.

402

403 **Conclusions**

404 Proximal outcrops through flood basalt flow fields and tephra deposits in the northwest USA, and
405 tephra deposits from modern and historic basaltic eruptions on Iceland and Tenerife, illustrate how

406 once-continuous tephra fall deposits can become disrupted through movement of underlying lavas
407 emitted during the same eruption. The inferred range of lateral displacement in these examples
408 varies from metres to 100s metres, and the resultant structures vary from extended (rifted) sheets
409 through to isolated mounds and ridges. In the Roza Member, CRBG, and at Chinyero, Tenerife,
410 proximal tephra sheets have been disrupted on top of pāhoehoe sheet lobes that were inflating
411 during and following fall out. Lateral and vertical movement of the upper crust of the pāhoehoe
412 flow resulted in the formation of mounds of tephra. In the Grande Ronde Member, CRBG, squeeze-
413 ups from active lava flows have intruded into overlying tephra fall deposits from the same eruption.
414 Leakage of lava out of the upper crust of inflating pāhoehoe lava flows up through overlying tephra
415 deposits can result in complicated stratigraphic relationships. At Hekla, Iceland, downslope creep in
416 a clastogenic lava led to the rifting apart of overlying non-welded tephra fall deposit to form a series
417 of steep-sided ridges and fissures. We recommend that the sorts of structures and field relationships
418 presented here for proximal environments for basaltic eruptions should be sought out and avoided
419 when collecting data for isopach or isopleth maps. Disruption of tephra sheets can result in
420 modification of the original deposit thickness, and to allochthonous outcrops of tephra, to
421 diachronous and complicated relationships between coeval tephra fall deposits and lavas. These
422 complexities may remain cryptic in the field due to the common textural, physical, and geochemical
423 similarity of lavas and of tephra deposits emplaced during any one basaltic eruption.

424

425 **Acknowledgements**

426 Research in the CRBG was funded by a Natural Environment Research Council Standard Grant
427 (NE/E019021/1) awarded to S. Self. T. Thordarson was partly funded by NASA and the University
428 of Hawai‘i. We thank C. Parcheta and S. Rowland for positive and constructive reviews and M.
429 Patrick for editorial assistance and advice.

430

431 **References**

432 Barry TL, Self S, Kelley SP, Reidel S, Hooper P, Widdowson M (2010) New $^{40}\text{Ar}/^{39}\text{Ar}$ dating of
433 the Grande Ronde lavas, Columbia River basalts, USA: Implications for duration of flood basalt
434 eruption episodes. *Lithos* 118:213-222

435

436 Bonadonna C, Houghton BF (2005) Total grain-size distribution and volume of tephra fall deposits.
437 *Bull Volcanol* 67:441-456

438

439 Branney MJ, Kokelaar P (2002) Pyroclastic density currents and the sedimentation of ignimbrites.
440 *Geol Soc London Memoir* 27:1-152

441

442 Brown RJ, Blake S, Thordarson T, Self S (2014) Eruption processes, pyroclastic deposits and
443 volcanic edifices of flood basalt fissure eruptions (The Roza Member, Columbia River Basalt
444 Province, US). *Geol Soc Am Bull* 126:875-891

445

446 Carey S, Sparks RSJ (1986) Quantitative models of the fallout and dispersal of tephra from volcanic
447 eruption columns. *Bull Volcanol* 48:109-125
448

449 Carracedo JC (2013) The Last 2 ky of Eruptive Activity of the Teide Volcanic Complex: Features
450 and Trends. In: Carracedo JC, Troll VR (eds) *Teide Volcano*. Springer Berlin Heidelberg 129-153
451

452 Carracedo JC, Rodriguez Badiola E, Solera V (1992) The 1730–1736 eruption of Lanzarote, Canary
453 Islands: a long, high-magnitude basaltic fissure eruption. *J Volcanol Geotherm Res* 53:239–250
454

455 Duraiswami RA, Bondre NR, Managave S (2008) Morphology of rubbly pāhoehoe (simple) flows
456 from the Deccan volcanic province: Implications for style of emplacement. *J Volcanol Geotherm*
457 *Res* 177:822-836
458

459 Fedotov SA, Chirkov AM, Gusev NA, Kovalev GN, Slezin Yu B (1980) The large fissure eruption
460 in the region of Plosky Tolbachik volcano in Kamchatka, 1975–1976. *Bull Volcanol* 43:47-60
461

462 Guilbaud M-N, Self S, Thordarson T, Blake S (2005) Morphology, surface structures, and
463 emplacement of lavas produced by Laki, A.D. 1783-1784. *Geol Soc Am Special Paper* 396:81-102
464

465 Gudmundsson A, Oskarsson N, Gronvold K, Saemundsson K, Sigurdsson O, Stefansson R,
466 Gislason SR, Einarsson P, Brandsdottir, B, Larsen, G, Johannesson, H, Thordarson, T (1992) The
467 1991 eruption of Hekla, Iceland. *Bull Volcanol* 54:328-246
468

469 Heliker C, Kauahikaua J, Sherrod DR, Lisowski M, Cervelli P (2003) The rise and fall of Pu‘u ‘Ō‘ō
470 Cone, 1983-2002. In: Heliker C, Swanson DA, Takahashi TJ (eds) *Pu‘u ‘Ō‘ō -Kūpāinaha eruption,*
471 *Kīlauea volcano, Hawai‘i: the first 20 years*. USGS Prof Paper 1676:29-52
472

473 Holm RF (1987) Significance of agglutinate mounds on lava flows associated with
474 monogenetic cones: an example at Sunset Crater, northern Arizona. *Geol Soc Am Bull* 99:319–324.
475

476 Hon K, Kauahikaua J, Denlinger R, Mackay K (1994) Emplacement and inflation of pāhoehoe
477 sheet flows: observations and measurements of active lava flows on Kīlauea volcano, Hawai‘i. *Geol*
478 *Soc Am Bull* 106:351–370
479

480 Houghton BF, Bonadonna C, Gregg CE, Johnston DM, Cousins WJ, Cole JW, Del Carlo P (2006)
481 Proximal tephra hazards: Recent eruption studies applied to volcanic risk in the Auckland volcanic
482 field, New Zealand. *J Volcanol Geotherm Res* 155:138-149
483

484 Keszthelyi L, Thordarson T, McEwen A, Haack A, Guilbaud MN, Self S, Rossi MJ (2004)
485 Icelandic analogs to Martian flood lavas. *Geochem Geophys Geosys* Q11014 DOI:
486 10.1029/2004GC000758
487

488 Lopez T, Thomas HE, Prata AJ, Amigo A, Fee D, Moriano D (2014) Volcanic plume
489 characteristics determined using an infrared imaging camera. *J Volcanol Geotherm Res* 300:148-
490 166
491

492 Martin BS (1989) The Roza Member, Columbia River Basalt Group: Chemical stratigraphy
493 and flow distribution. In: Reidel SP, Hooper PR (eds) *Volcanism and tectonism in the Columbia*
494 *River flood basalt province*: *Geol Soc Am Spec Paper* 239:85–104
495

496 Parcheta CE, Houghton BF, Swanson DA (2012) Hawaiian fissure fountains 1: decoding deposits—
 497 episode 1 of the 1969–1974 Mauna Ulu eruption. *Bull Volcanol* 74:1729-1743
 498

499 Parfitt EA, Wilson L (1999) A Plinian treatment of fallout from Hawaiian lava fountains. *J*
 500 *Volcanol Geotherm Res* 88:67-75
 501

502 Passmore E, Maclennan J, Fitton G, Thordarson T (2012) Mush disaggregation in basaltic magma
 503 chambers: evidence from the AD 1783 Laki eruption. *J Pet* 53:2593-2623
 504

505 Pioli L, Azzopardi BJ, Cashman KV (2009) Controls on the explosivity of scoria cone eruptions:
 506 Magma segregation at conduit junctions. *J Volcanol Geotherm Res* 186:407-415 DOI:
 507 10.1016/j.jvolgeores.2009.07.014
 508

509 Pyle DM (1989) The thickness volume and grainsize of tephra fall deposits. *Bull Volcanol* 51:1-15
 510

511 Richter DH, Eaton JP, Murata KJ, Ault WU, Krivoy HL (1970) Chronological narrative of the
 512 1959–60 eruption of Kīlauea volcano, Hawai‘i. In: The 1959–60 eruption of Kīlauea volcano,
 513 Hawai‘i. *US Geol Surv Prof Pap* 537-E:E1–E73
 514

515 Riggs NR Duffield WA (2008) Record of complex scoria cone eruptive activity at Red Mountain,
 516 Arizona, USA, and implications for monogenetic mafic volcanoes. *J Volcanol Geotherm Res*
 517 178:763–776
 518

519 Rowland SK, Jurado-Chichay Z, Ernst G, Walker GPL (2009) Pyroclastic deposits and lava flows
 520 from the 1759–1774 eruption of El Jorullo, Mexico: aspects of ‘violent Strombolian’ activity and
 521 comparison with Parícutin. In: Thordarson T, Self S, Larsen G, Rowland SK, Hoskuldsson A (eds)
 522 *Studies in Volcanology: The Legacy of George Walker*. Special Publications of IAVCEI, Geol Soc
 523 London 2:105–128
 524

525 Self S, Widdowson M, Thordarson T, Jay AE (2006) Volatile fluxes during flood basalt eruptions
 526 and potential effects on the global environment: A Deccan perspective. *Earth Planet Sci Lett*
 527 248:518-532
 528

529 Sigmarsson O, Condomines M, Gronvold K, Thordarson T (1991) Extreme magma homogeneity in
 530 the Laki 1783-84 Lakagigar eruption: origin of a large volume of evolved basalt in Iceland.
 531 *Geophys Res Lett* 18:2229-2232
 532

533 Swanson DA, Wright TL, Helz RT (1975) Linear vent systems and estimated rates of magma
 534 production and eruption for the Yakima basalt of the Columbia plateau. *Am J Sci* 275:877-905
 535

536 Thordarson T, Self S (1993) The Laki (Skaftár Fires) and Grímsvötn eruptions in 1783–1785. *Bull*
 537 *Volcanol* 55:233–263
 538

539 Thordarson T, Self S (1996) Sulfur, chlorine and fluorine degassing and atmospheric loading by the
 540 Roza eruption, Columbia River Basalt Group, Washington, USA. *J Volcanol Geotherm Res* 74:49-
 541 73
 542

543 Thordarson T, Self S (1998) The Roza Member, Columbia River Basalt Group: a gigantic pāhoehoe
 544 lava flow field formed by endogenous processes. *J Geophys Res* 103:27,411-27,445
 545

546 Valentine GA, Perry FV, Krier D, Keating GN, Kelley RE, Coghill AH (2006) Small-volume
547 basaltic volcanoes: Eruptive products and processes, and post-eruptive geomorphic evolution in
548 Crater Flat (Pleistocene), southern Nevada. *Geol Soc Am Bull* 118:1313-1330
549

550 Vye-Brown C, Gannoun A, Barry TL Self S, Burton KW (2013) Osmium isotope variations
551 accompanying the eruption of a single lava flow field in the Columbia River Flood Basalt Province.
552 *Earth Planet Sci Lett* 368:183-194
553

554 Walker GPL (1991) Structure, and origin by injection of lava under surface crust, of tumuli, "lava
555 rises", "lava-rise pits", and "lava-inflation clefts" in Hawaii. *Bull Volcanol* 53: 546–558
556

557 Wilson L, Walker GPL (1987) Explosive volcanic eruptions - VI. Ejecta dispersal in Plinian
558 eruptions: the control of eruption conditions and atmospheric properties. *Geophys J Int* 89:657-679
559

560 **Figure captions**

561 **Figure 1.** Geological sketch map of pyroclastic deposits at the northern end of the Roza vent
562 system, CRBG (modified from Brown et al. 2014).
563

564 **Figure 2.** Interpretations of man-made cuts through the Roza Member at Winona (Table 1),
565 illustrating how a tephra fall deposit has been dissected into a number of mounds and the complex
566 stratigraphic relationships between pyroclastic rocks and lavas. The mounds have been draped by
567 later welded spatter and tephra fall deposits. The inferred vent for the pyroclastic deposits lies ~500
568 m towards the east of the illustrated rail cut. For location see Figure 1. White rectangles show
569 locations of Figures 3A and 3C. Scale applies to all parts.
570

571 **Figure 3.** A) Typical mound of tephra in the Roza Member at Winona. Mound consists of a well-
572 sorted, massive tephra fall deposit and overlies rubbly vesicular pāhoehoe crust in which lapilli fill
573 the voids between slabs and blocks of crust. The mound is draped by welded fall deposits that have
574 welded the clasts on the exterior of the mound. Metre rule for scale. See Fig. 2 for location. B)
575 Upturned slab of vesicular pāhoehoe crust at the base of a tephra mound. See Fig. 1 for location.
576 Metre rule for scale. C) Photograph and interpretive sketch of intercalated pāhoehoe lava and tephra
577 within a mound at Winona (see Fig. 1 for location). Mound 1 overlies rubbly pāhoehoe , as in B,
578 and is in turn buried by lava (2). Lava 2 is overlain by a second tephra fall deposit, which has also
579 been modified into a mound. This second mound has been draped by welded fall deposits and is
580 buried beneath lava 3. A crack developed through the tephra deposits has been filled by lava 3.
581 Lava 2 may have been fed by a breakout from a tumulus in lava 1. See Fig. 2 for key.
582

583 **Figure 4.** Lava intrusions in a tephra fall deposit fed by breakouts from an underlying inflating lava
584 flow of the Grande Ronde lavas, CRBG. A) Sketch of roadcut showing irregular intrusions cutting
585 through a thick tephra fall deposit. Margins of the intrusions are locally brecciated and have
586 thermally altered the host deposit. Intrusions strike nearly parallel to the roadcut. Vent location for
587 the tephra deposits is not known. B) Stubby intrusion showing dense interior with large gas cavities.
588 Note thermal alteration (orange oxidation) of host rock. C) Multiple intrusions with brecciated
589 margins (right) and thermal alteration. Intrusion on left appears to taper upwards. Inset map shows
590 location (asterisk; see also Table 1); extent of CRBG lavas shown in grey shade.
591

592 **Figure 5.** Interpreted satellite image of the 1909 Chinyero scoria cone and erupted products,
593 Tenerife. Scoria fall deposit south of the scoria cone has rifted apart on top of lava flows. Arrows
594 show main lava pathways. Image from GoogleTM Earth Pro.
595

596 **Figure 6.** Dissected tephra fall deposits of the 1909 eruption of Chinyero, Tenerife. A) View east
 597 from the Chinyero scoria cone showing how the proximal tephra sheet has been transported and
 598 disrupted into mounds on top of a rubbly lava flow. Distal parts of the tephra sheet have been over-
 599 ridden by the lava. B) Detail of disrupted tephra mounds. Note similarity to those in Figures 2 and
 600 3. C) Tephra blanket on right of photo is inferred to be the same age as that on the left, which has
 601 been transported from a more proximal position on top of lava. D) Remnants tephra fall deposit on
 602 main lava flow from the Chinyero eruption situated west of the main cone (see Fig. 5 for location).
 603 Note large rafted blocks of scoria cone in distance.
 604

605 **Figure 7.** Geological sketch map of the products of the 1991 eruption of Hekla, Iceland. Modified
 606 from Gudmundsson et al. (1992).
 607

608 **Figure 8.** Disrupted tephra fall deposits of the 1991 eruption of Hekla, Iceland. A) Aerial
 609 photograph of the East Cone and disrupted fall deposit. Arrows indicate downhill slope direction.
 610 B) Extensional fissures in the disrupted tephra fall deposit. C) Deep fissures exposing coarse-
 611 grained spatter. Bag for scale. Line marks base of non-welded tephra. D) Rotated block within
 612 extensional fissure.
 613

614 **Figure 9.** Cartoon illustrating the disruption of a sheet-form tephra fall deposit into partially
 615 connected mounds by the inflation and lateral spread of a subjacent lava flow. Breakouts may flow
 616 across the surface of tephra deposits or may intrude into overlying fall deposits. Inset shows tephra
 617 deposit prior to disruption.
 618

619 **Figure 10.** Cartoon to illustrate the hypothetical diachronous relationships between a synchronously
 620 emplaced lava flow and a tephra fall deposit in vent-proximal regions. Relationships are likely to
 621 remain cryptic due to the common physical, textural and chemical homogeneity of basaltic fall
 622 deposits, and to complex lava pathways.
 623

624 **Table 1.** Localities of key examples of the features described in the text.
 625

Feature	Location	Country	Grid reference
Dissected tephra fall deposits	Winona	Washington, USA	46°56'36.17"N 117°47'37.31"W
	Little Sheep Creek	Oregon, USA	45°20'8.15"N 117° 4'48.61"W
	Chinyero	Tenerife, Spain	28°17'39.76"N 16°45'16.53"W
	Laki (Hnúta)	Iceland	64°00'21.39"N 18°22'28.71"W
	Laki (Varmárdalur)	Iceland	64°02'24.11"N 18°16'47.65"W
	Hekla	Iceland	63°59'18.09"N 19°38'12.38"W
Intercalated lava and tephra	Winona	Washington, USA	46°56'35.11"N 117°48'22.05"W
	Lancaster Road	Washington, USA	46°57'28.31"N 117°48'30.66"W
Rafted tephra deposits	Mason Draw	Washington, USA	46°57'33.59"N 117°51'9.35"W
	Winona	Washington, USA	46°56'15.49"N 117°49'33.62"W
	Palouse River	Washington, USA	46°55'10.77"N 117°51'7.37"W
	Chinyero	Tenerife, Spain	28°17'28.66"N 16°45'25.75"W

626
 627 **Table 2.** Physical characteristics of the tephra mounds in 2-D man-made cuts through the Roza
 628 Member at Winona (Fig. 1). d – spacing, centre to centre of mound from left to right; h – height; w
 629 – width; Θ – mean slope angle. *Minimum values.
 630

d (m)	h (m)*	w (m)*	Θ	morphology
-	4	20	24°	double peaked
41	2	13	27°	peaked
26	5	8	36°	rounded
35	2.5	30	20°	flat/rounded

35	4	16	24°	flat topped
36	2.5	6	34°	peaked
20	4	20	24°	flat-topped

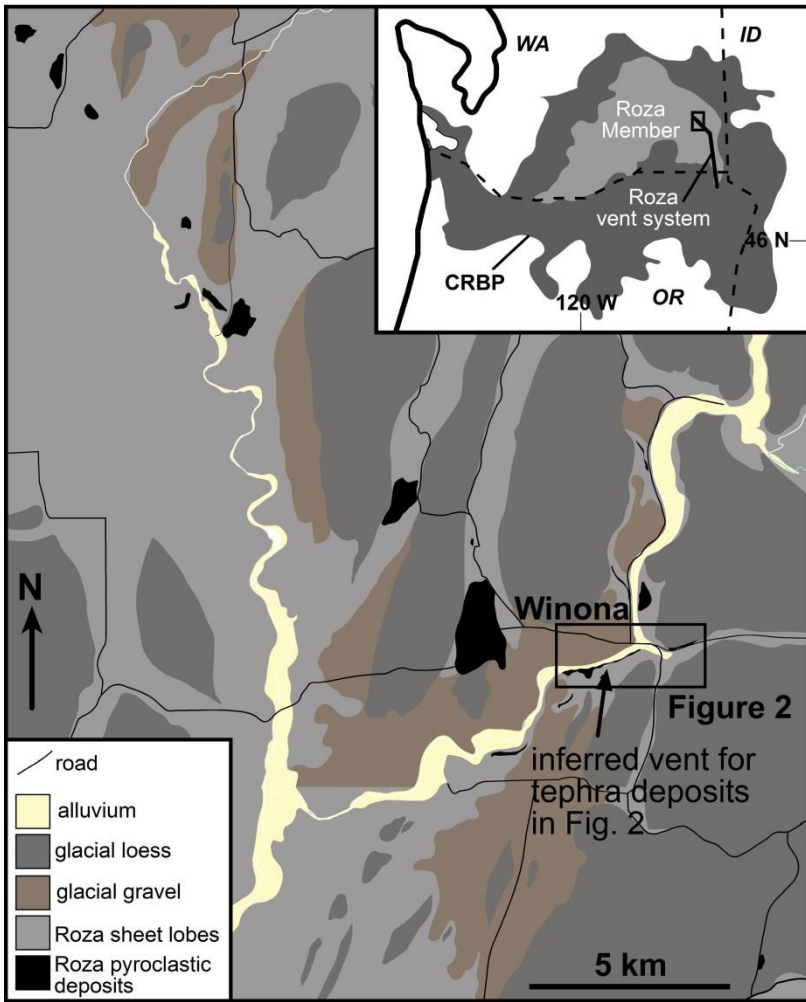
631

632 **Table 3.** Physical characteristics of tephra mounds on the north portion the Chinyero lava flow,
 633 Tenerife. h – height; w – width; Θ – mean slope angle.

634

h (m)*	w (m)*	Θ	morphology
2	5	20°	peaked
2	8	22°	double peaked
1	3	36°	peaked
2.5	6	32°	peaked
2.5	25	32°	hummocky
<1	3	36°	peaked
<1	4.5	21°	flat topped

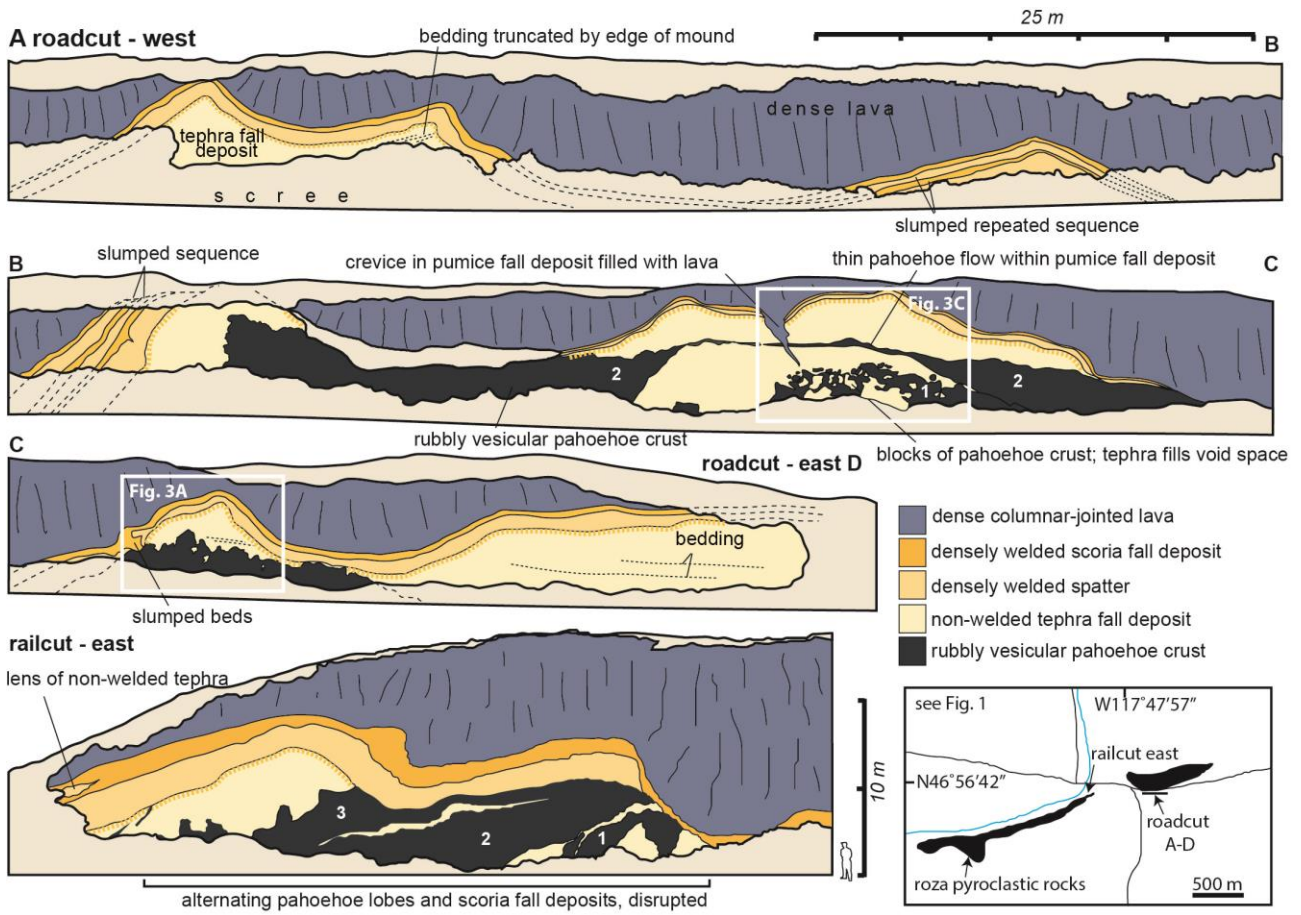
635



1
2
3
4
5
6
7
8
9
10
11
12
13
14
15
16
17
18
19
20
21
22
23
24

Fig 1

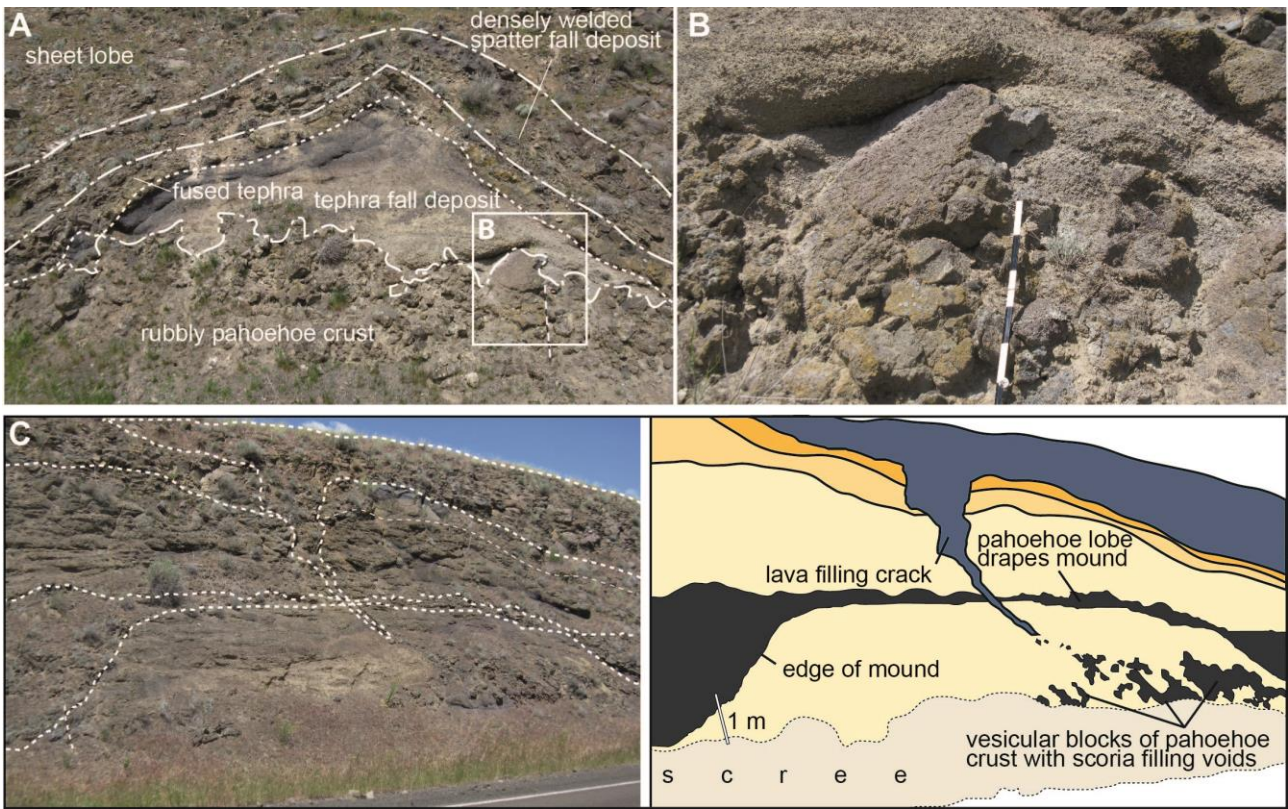
25
26



27
28
29
30
31
32
33
34
35
36
37
38
39
40
41
42
43
44
45
46
47
48
49
50
51

Fig 2

52
53

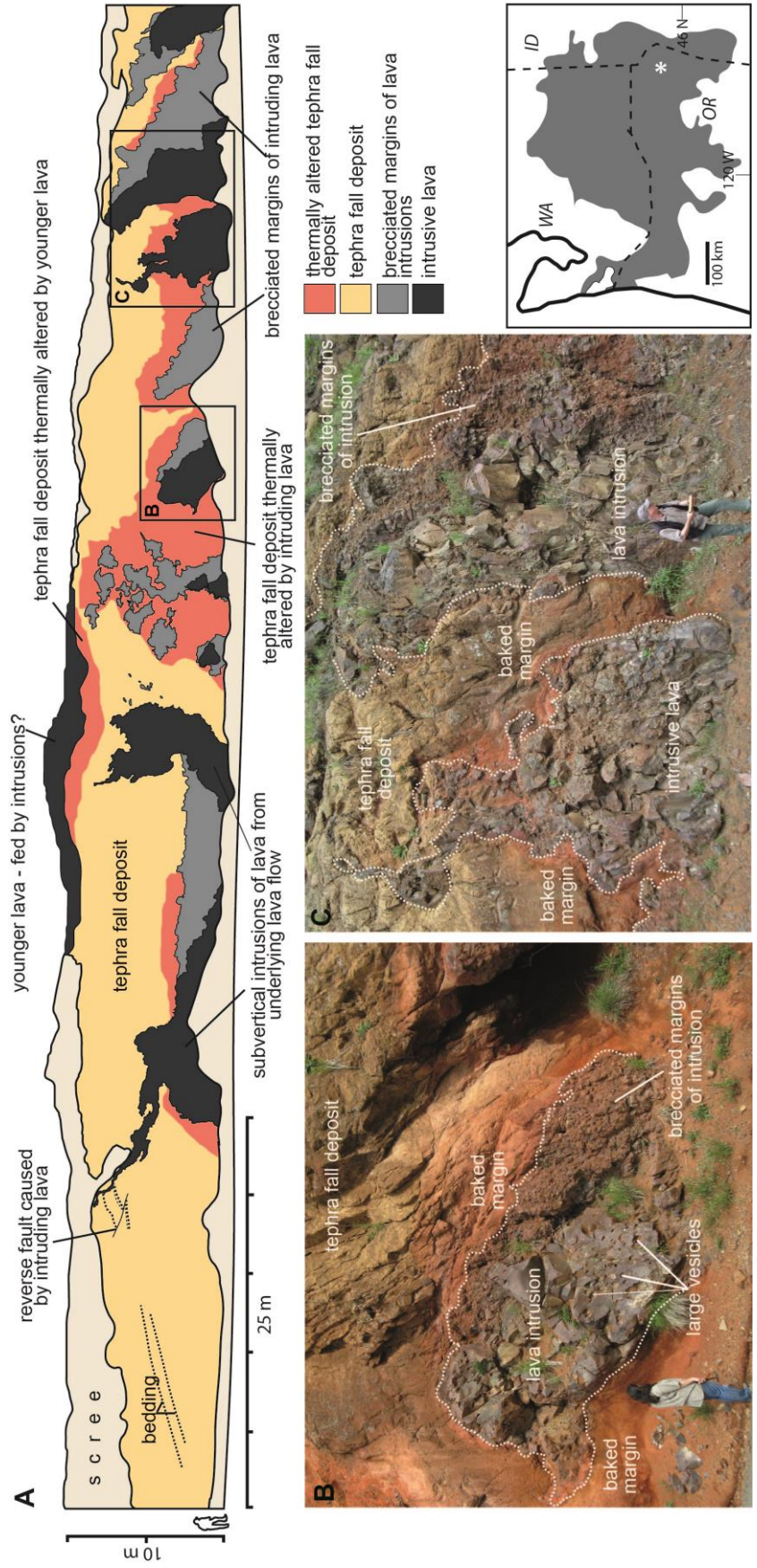


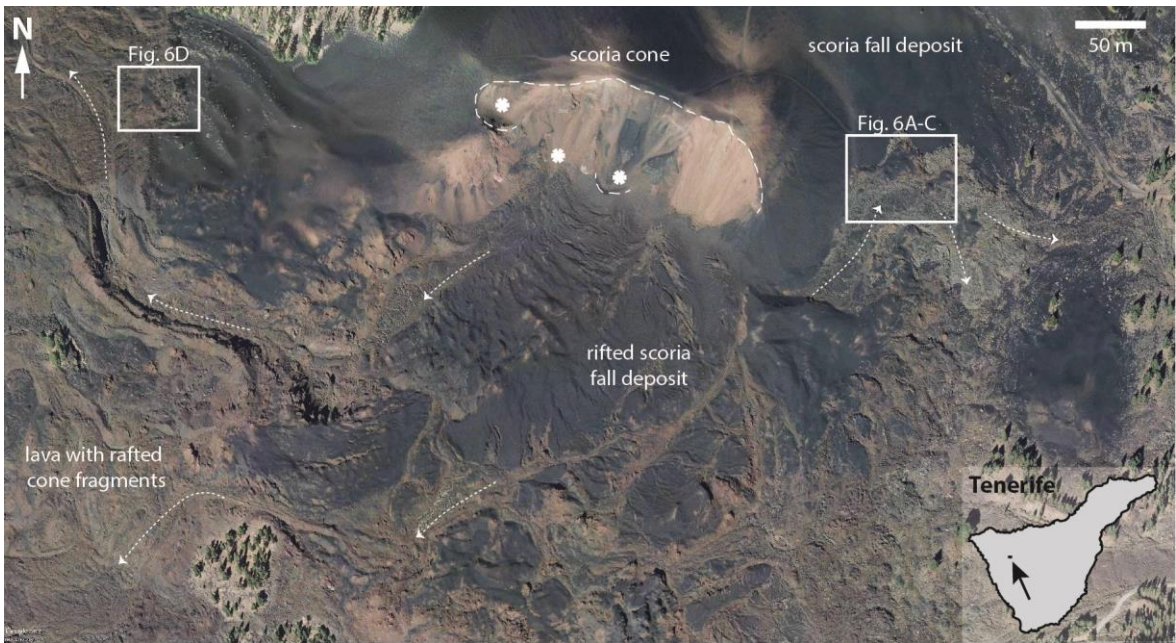
54
55
56

Fig 3

57
58
59
60

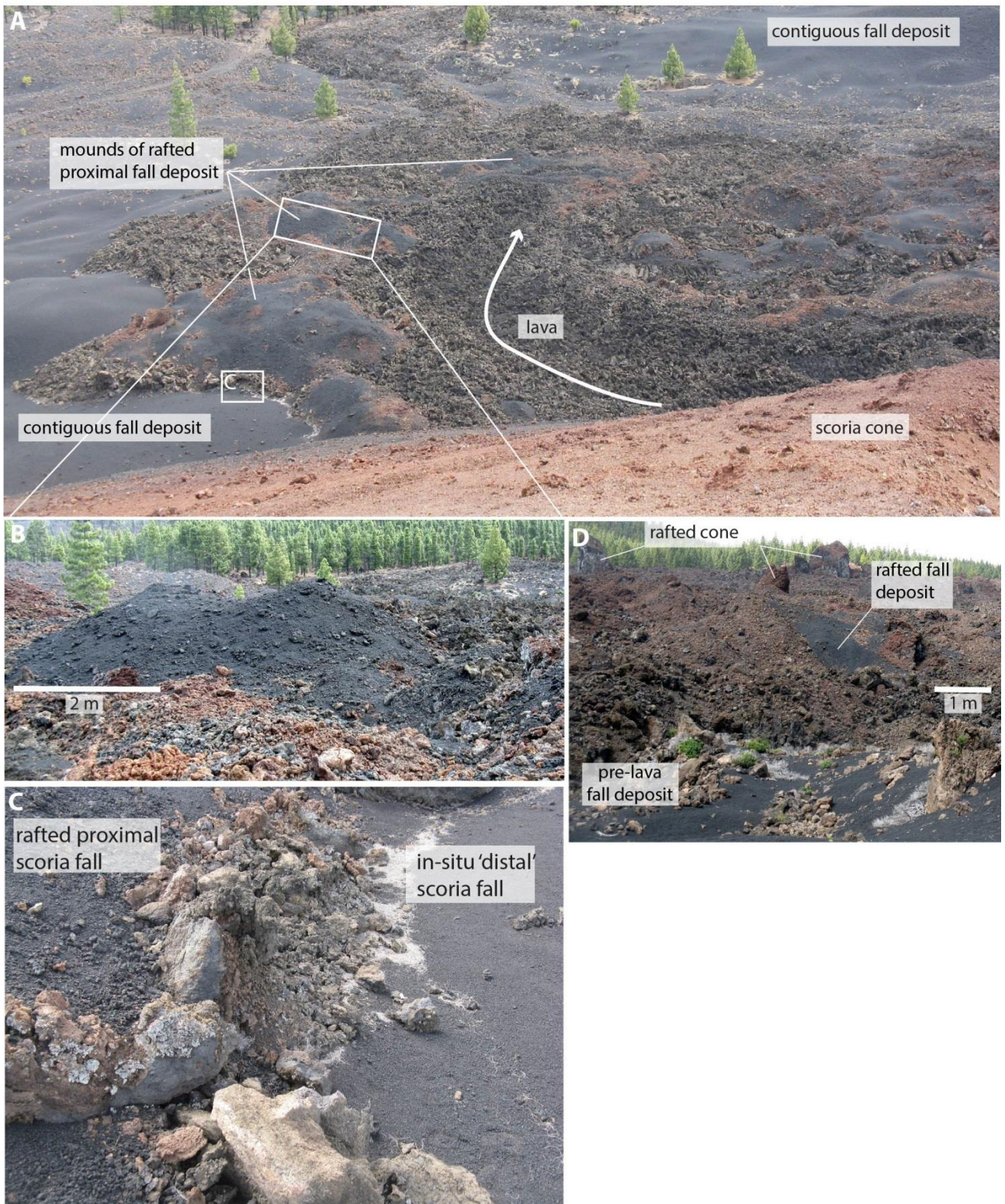
Fig 4





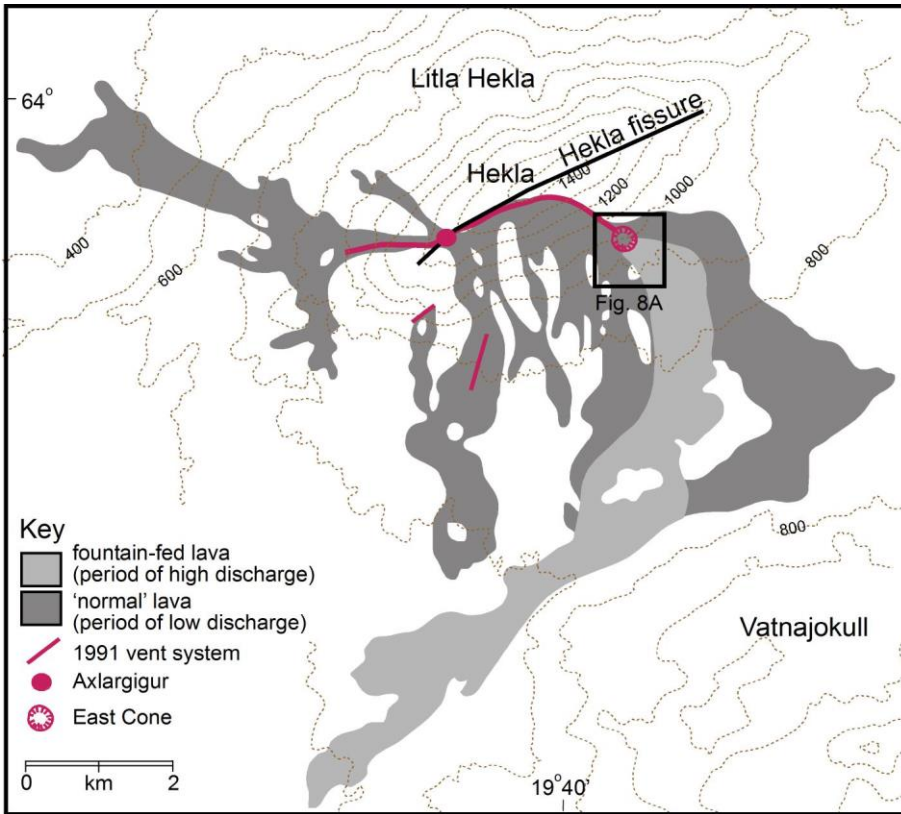
61
62
63
64
65
66
67
68
69
70
71
72
73
74
75
76
77
78
79
80
81
82
83

Fig 5



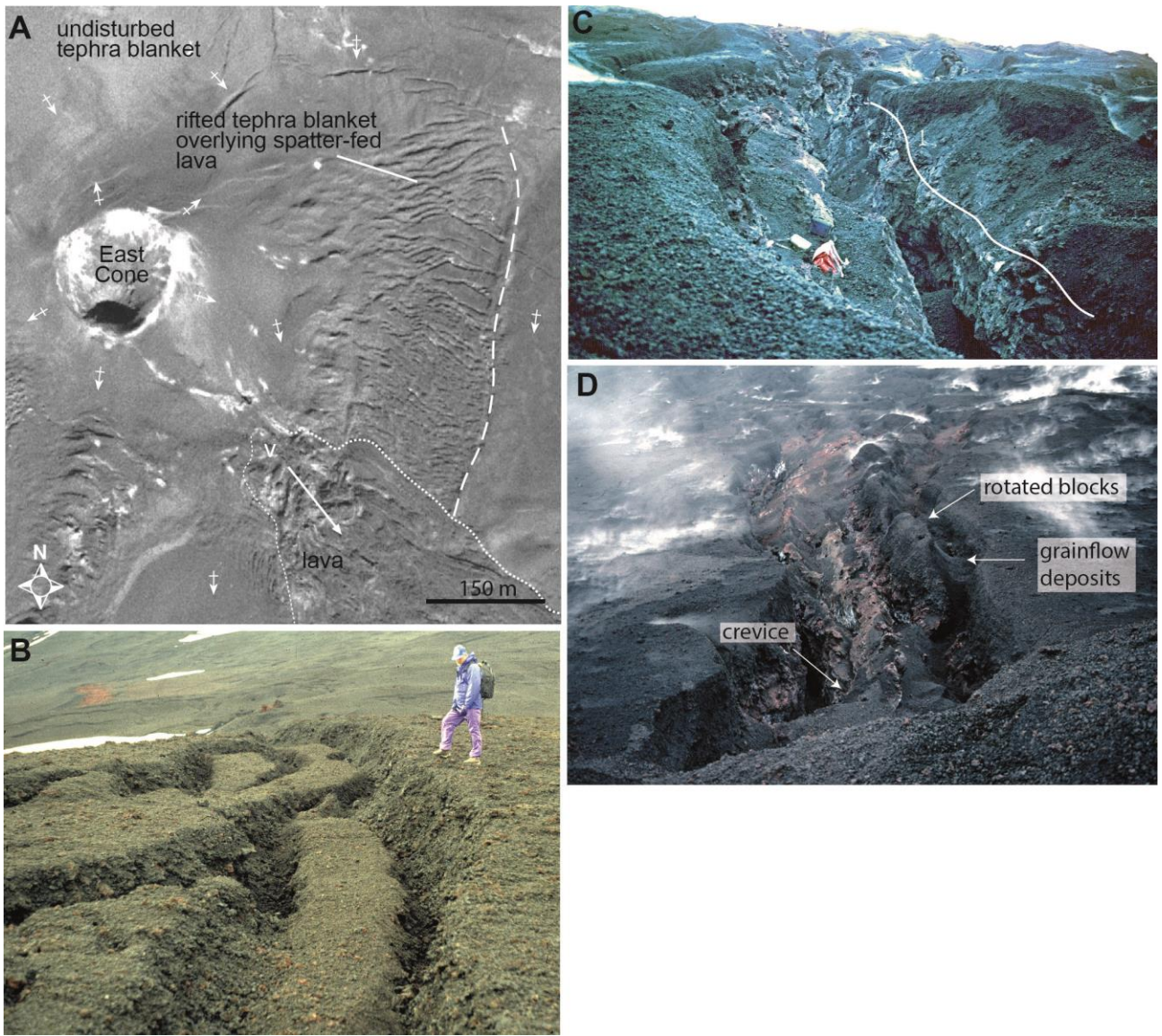
84
85
86
87
88

Fig 6



89
 90
 91
 92
 93
 94

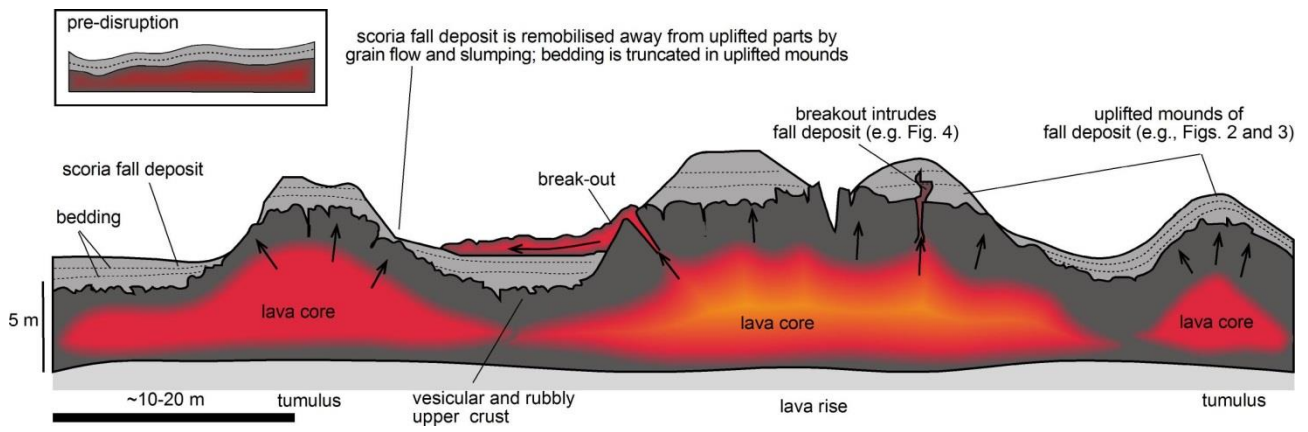
Fig 7



95
 96
 97
 98
 99
 100
 101
 102
 103
 104
 105
 106
 107
 108
 109
 110
 111
 112
 113
 114

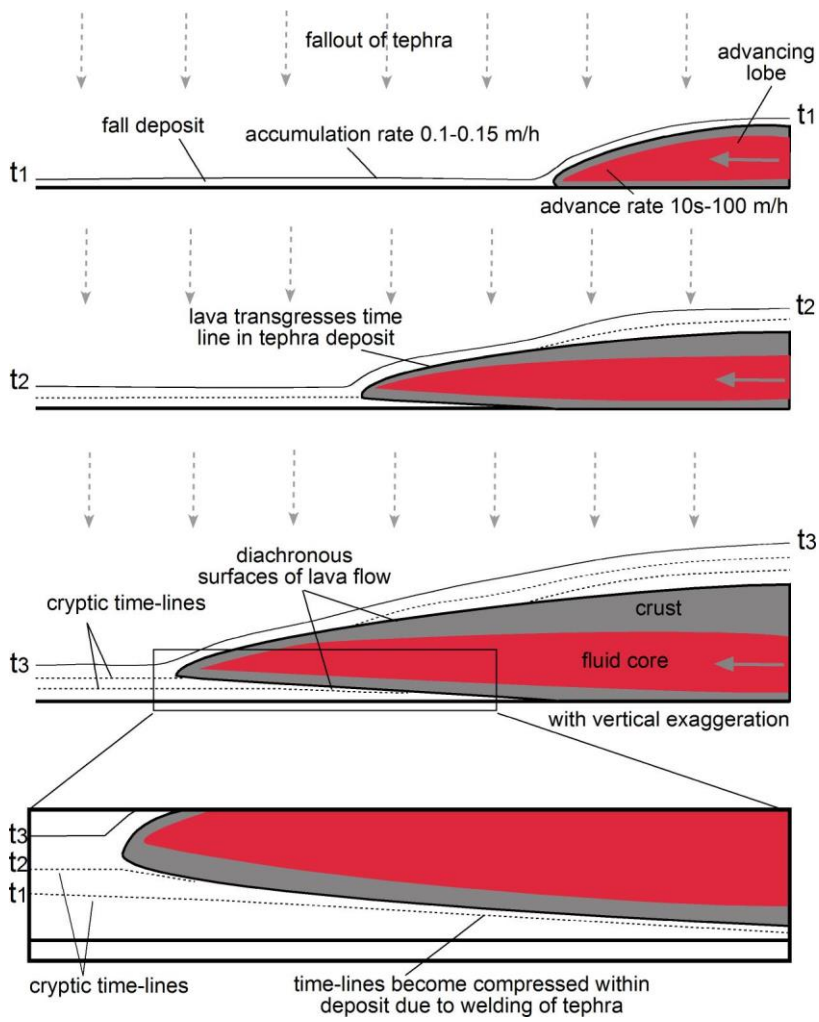
Fig 8

115
116
117
118



119
120
121
122
123
124
125
126
127
128
129
130
131
132
133
134
135
136
137
138
139
140
141
142
143
144
145
146
147
148
149
150
151
152
153

Fig 9



154
155
156
157

Fig 10